Investigation of Landsat-4 Thematic Mapper Line-to-Line and Band-to-Band Registration and Relative Detector Calibration

Jacky Desachy
Laboratoire C.E.R.F.I.A., Université Paul Sabatier (UER MIG), 118 Route de Narbonne, 31062 Toulouse Cedex, France

Gérard Begni, Benoit Boissin, and *Jacqueline Perbos*
Centre National d'Etudes Spatiales, PMF/TI/AS, 18 Avenue Edouard Belin, 31055 Toulouse Cedex, France

ABSTRACT: Our objectives in this study were to test Landsat-4 TM geometric and radiometric characteristics and more precisely line-to-line and band-to-band registration problems, detector-to-detector relative calibration, and within-line bright target saturation. Correlation techniques were used to find the best matching between two zones of two different lines (or bands) and by using Lagrange polynomials, we reached a 0.1 IFOV accuracy. Analysis of statistically significant results is presented in comparison to TM physical specifications. A detector calibration method is applied, based upon a histogram matching principle. Look-up tables are computed for each detector with regard to mean detector. Nonlinearities in detectors' responses can be estimated and a destriped image constructed. Our method is applied to various images in order to detect whether radiometric accuracy specifications are met. The special case of bright target saturation is analyzed for snow-covered regions. Mean detector responses for forward and reverse scans are computed in order to evaluate the saturation level and recovery time. Computed intraband misregistrations for P-type images agree with specifications, but we found that significant misregistrations are near columns 1500 and 4500. In A-type images and in P-type images, we found significant misregistrations between bands of different focal planes and between band 6 and others. Concerning radiometric calibration, we found two detectors dead, and some detectors are under TM specifications (especially in bands 1, 2, 3, and 4). The bright target saturation is obvious in bands 1 and 2, and, detector's response recovery may last for thousands of pixels.

INTRODUCTION

OUR EXPERIENCE SHOWS that image quality parameters can have an important influence on the results of users' investigations, and that evaluation of the scanners delivering the images we use is of first importance. The defaults linked to the scanner itself can be partially corrected by a ground preprocessing. So, it is necessary to study the raw image quality to optimize the ground segment algorithms, then the preprocessed images quality so as to characterize the products delivered to users. That was precisely the goal of NASA's LIDQA Program concerning in particular the innovative TM scanner.

Our study is restricted to Thematic Mapper and is concerned with: (1) evaluation of intraband line-to-line misregistrations and interband misregistrations for both A-type and P-type images, and (2) detector calibration and the related bright target saturation problem.

This analysis has been performed on the following scenes:

- Landsat TM A-type scene of Toulouse (France) (Scene 198/30 of 23 January 1983)
- Landsat TM A-type scene of Mississippi (22 August 1982)
- Landsat TM P-type scene of Mississippi (22 August 1982)
- Landsat TM A-type scene of Lukeville (15 January 1983)

Our investigation has been performed on the Centre National d'Etudes Spatiales's CDC computer.

LINE-TO-LINE AND BAND-TO-BAND REGISTRATION

METHODOLOGY

The method we use is based on automatic correlation techniques and proceeds on a line-by-line basis (intraband line-to-line registration or inter-

PHOTOGRAMMETRIC ENGINEERING AND REMOTE SENSING, Vol. 51, No. 9, September 1985, pp. 1291-1298.

0099-1112/85/5109-1291$02.25/0

band registration for one given line), as described by Jeansoulin (1980).

Our problem is to store the existing pixel offsets, from one line to the other, all along one line. To achieve this, we first isolate the two concerned lines (the two consecutive lines in the case of line-to-line misregistration estimation, the two corresponding lines in each band in the band-to-band misregistration estimation). We divide these two lines into nine overlapping segments (1025 pixels long). For each segment pair (one segment from each line, let us call them X and Y arrays, each consisting of 1025 pixels), we carry out the following process:

We choose a 512-pixel segment centered on Y (1025 pixels) and shift this 512-pixel segment along a segment N_c pixels long ($N_c > 512$) centered on X (1025 pixels). We then compute the $N_c - 511$ correlation function values between the two segments. (For example if $N_c = 652$, we are able to show a misregistration of up to $\pm$ 70 pixels).

$$R(l) = \frac{\sum_{i=256}^{767} (Y(i) - \overline{Y}) * (X(i + 1) - \overline{X}_l)}{\left(\sum_{i=256}^{767} (Y(i) - \overline{Y})^2 * \sum_{i=256}^{767} (X(i + 1) - \overline{X}_l)^2 \right)^{1/2}} \quad (1)$$

where:

$$\overline{X}_l = \frac{1}{512} \sum_{i=256}^{767} X(i + l) \quad \overline{Y} = \frac{1}{512} \sum_{i=256}^{767} Y(i) \quad (2)$$

and:

$$l = 0, \pm 1, \pm 2, \ldots, \pm (N_c - 512)/2 \quad (3)$$

Let l_{max} be the discrete value of l for which $R(l)$ is a maximum. Then by Lagrange polynomial interpolation we find the integer ϵ, such that $R(l_\epsilon)$ is a maximum with $l_\epsilon = l_{max} + 0.05\,\epsilon - 20 \leq \epsilon \leq 20$. A misregistration of 0.05 pixels may be detected by this method.

Results

Intraband Misregistrations. We looked first for intraband forward-reverse scan misregistrations. Mississippi A-type image line-ends (first or last pixel of one line) misregistrations vary from -45 to -49.1 pixels between reverse and forward scans and from 43.65 to 47.25 pixels between forward and reverse scans for bands 1 to 5 and for band 7 (respectively -36.5 to -43.95 and 39.95 to 43.9 for band 6).

Given this systematic misregistration of about 46 pixels between consecutive scans in raw images, there appears to be no systematic variation around that value.

On the Mississippi P-type image, however, line-end misregistrations between forward and reverse scans are below 0.3 pixels 99 percent of the time. On the other hand, we looked for variations between odd and even detectors for one given band: for A-type images, we found that the misregistrations between odd and even detectors are positive, and between even and odd detectors are negative, which is correlated with relative detectors' position.

As one can see on Table 1 the percentage of line-to-line misregistrations located between -0.3 and 0.3 pixel is always greater than 90 percent for all bands in both A-type and P-type images, in agreement with specifications. However, we made the following findings: (note that in Figure 1 and in the following remarks, the only misregistrations we shall talk about are those which are located between -0.3 and 0.3 pixel, and we excluded the case of line-to-line registration for two successive scans).

A-type Mississippi image

Band 1: Most misregistrations are found around columns 1500 and 4500.

Band 2: Most misregistrations are near columns 1500 and 4500 and are between detectors n°3 and 2 and between detectors n°2 and 1.

Band 3, band 4: Most misregistrations are near columns 1500 and 4500.

Band 5: Most misregistrations are near columns 1500 and 4500 and are between detectors n°8 and 7 and between detectors n°7 and n°6.

Band 6, band 7: Most misregistrations are near columns 1500 and 4500.

P-type Mississippi image

Band 1, band 2, band 3, band 4, band 5, band 7: Most misregistrations are near column 4500. The fact that in most cases, most significative misregistrations appear near columns 1500 and 4500 is probably related to the mirror scan angle.

Band-to-Band Registration. In this section we discuss misregistrations between different bands.

Table 1. Percentages of Intraband Detector Misregistration whose Absolute Value is Less than 0.3 Pixel for Mississipi Image (Excluding Interscan Misregistrations)

Bands	Band 1	Band 2	Band 3	Band 4	Band 5	Band 6	Band 7
A-Type Scene (percent)	96	90	98	99	95	97	97
P-Type Scene (percent)	97	97	97	98	96	99	97

We present results for the Toulouse raw image (this image has been preprocessed by Telespazio Center *in order to rectify forward-reverse scan misregistrations* by global translation by a whole number of pixels) and for the Mississippi A-type and P-type images.

We will now give results concerning misregistration statistics between different bands (Table 2 for the Toulouse image, Table 3 for the Mississippi A-type scene, and Table 4 for the P-type image). We will report these results as a percentage within a given level of misregistration and not as the usual average misregistration. Note that within each focal plane the interband misregistrations are within the designed specifications for all images (with no significant difference between A-type and P-type images for the primary focal plane bands). The results in Tables 2 and 3 show significant misregistration between focal planes for A-type images, for the P-type image of Mississippi, and with band 6. Both facts have been reported previously by Bernstein (1984), Anuta (1984), and Wrigley (1984).

For the Mississippi P-type image, between bands 4 and 6, our correlation technique has given some spurious misregistration values so that we can only give a rough result: the values are near those of bands 1 and 6 Mississippi A-type image misregistrations which are very large. Moreover, for the Mississippi P-type image, we obtained the following bad results: between bands 4 and 5 and between bands 5 and 7, almost all misregistration values were from 1.0 to 2.0 pixels. In fact while the Mississippi A-type image does not show such remarkable misregistrations, we found that in the P-type image, all computations related to band 5 gave surprisingly high misregistration values. It seems that some band 5 lines have been lost, or the band 5 first line does not correspond to other band's first line.

TABLE 2. TOULOUSE A-TYPE IMAGE INTERBAND MISREGISTRATION STATISTICS

Bands	Misregistration Limits (absolute value, unit: band 1 IFOV)	Misregistrations Within Limits (percent)
1–2	≤0.2	91
	≤0.3	95
3–4	≤0.2	90
	≤0.3	98
4–5	≤0.4	65
	≤0.5	90
4–7	≤0.4	75
	≤0.5	86
	≤0.6	94
5–7	≤0.15	93
	≤0.2	99

TABLE 3. MISSISSIPI A-TYPE IMAGE INTERBAND MISREGISTRATION STATISTICS

Bands	Misregistration Limits (absolute value, unit: band 1 IFOV)	Misregistrations Within Limits (percent)
1–2	≤0.2	95
3–4	≤0.2	86
	≤0.3	91
5–7	≤0.2	97
1–6	≤4.	67
	≤5.	90
4–5	≤0.7	70
	≤0.8	90
4–7	≤0.6	56
	≤0.8	88
	≤0.9	96
6–7	≤4.	86
	≤4.5	94

DETECTOR CALIBRATION

METHODOLOGY

We studied the general problem of detector calibration and the related bright target saturation. We shall describe successively each method we implemented. The method we used for detector calibration was one of relative calibration and has been successfully used for destriping images from previous Landsat systems (also for the Meteosat system) and applies to the TM as well as to the MSS instruments. It is based on a histogram matching principle: as Landsat images are formed by interlacing n subimages (n = 16 or 4), each one corresponding to a single detector, the assumption is made that, for a large enough image, each subimage has the same probability distribution of scene radiance values. Variations in the histograms obtained from these subimages can thus be attributed to gain differences between the sensors. Detector equaliza-

TABLE 4. MISSISSIPI P-TYPE IMAGE INTERBAND MISREGISTRATION STATISTICS

Bands	Misregistration Limits (absolute value, unit: band 1 IFOV)	Misregistration Within Limits (percent)
3–4	<0.2	87
	≤0.2	95
	≤0.3	96
3–7	≤0.7	90
4–7	≤0.7	85
	≤0.8	94

tion (destriping) consists of superimposing the histograms.

We applied the general following method: let X be a random variable, with cumulative density function ($C_X(x)$. If we consider a random variable X' generated by $X' = f(X)$ it can be shown that

$$C_X(x) = C_{X'}[f(x)] \tag{4}$$

So, if we can compute $C_{X'}$, we can find f by

$$f(x) = C_{X'}^{-1}[C_X(x)] \tag{5}$$

For each detector j ($j = 1 \ldots 16$ for bands 1 to 5 and band 7 and $j = 1 \ldots 4$ for band 6) we can compute the histogram $HIST_j(n)$, $n = 0, \ldots, 255$.

By linear interpolation of the histograms, we can obtain good estimates of the continuous cumulative functions $HISCUM_j(x)$, $x \in [0,255]$. For the reference detector for calibration we use the mean detector for which we compute the cumulative density function $HCUMMOY(x)$, $x \in [0,255]$. Then for each detector j, and gray level k, we can compute a lookup table relative to the mean detector (see Figure 1).

$$k \rightarrow x_j(k) = HCUMMOY^{-1}(HISCUM_j(k)) \quad k = 0, \ldots, 255 \tag{6}$$

For practical purposes (see Tables 5, 6, and 7), we summarize the lookup table results by the mean relative calibration computed in the following form:

$$(n_2 - n_1 + 1)^{-1} \sum_{k=n_1}^{n_2} (x_j(k) - k) \tag{7}$$

n_1 and n_2 being chosen referring to a detector's density function $HIST_j$ significative part (nonzero density range). However, for each detector, the lookup table examination will give an idea of the nonlinearities that may occur in the sensor responses, in reference to mean sensor. The computed lookup tables can then be used for destriping images for it takes into account the fact that striping depends upon the observed spectral response.

We have also studied the problem of detector saturation for bright targets and the hysteresis effect in a detector's slow response recovery. We chose a snow field border in the Toulouse image and looked for the mean detector profile for pairs of consecutive forward-reverse scans. This showed the hysteresis effect in a detector's response and allowed us to estimate the detector's response recovery time along one line.

Results

Let us recall the TM specification: detector-to-detector differences within bands must be restrained to ± 1 quantum level. We tested the specification in the A-type Toulouse scene (Table 5), and the A-type Mississippi scene (Table 6) by analyzing the detector relative calibration. We checked whether the ± 1 quantum level specification was achieved by studying one special case of a homogeneous target (sea) in the A-type Lukeville scene (Table 7). At the end of this paper we shall discuss the bright target saturation and recovery for the A-type Toulouse image in band 1 for which this phenomenon is quite severe.

Relative Detector Calibration. First of all, we have established that except for the Toulouse A-type scene, the Mississippi and Lukeville scenes present gray level histogram discontinuities (certain digital numbers never appear) in all bands, caused by stretch in histogram (gain >1). On the Toulouse A-type scene we found that detector 3 of band 5 is dead, so we omitted it in our computations with this

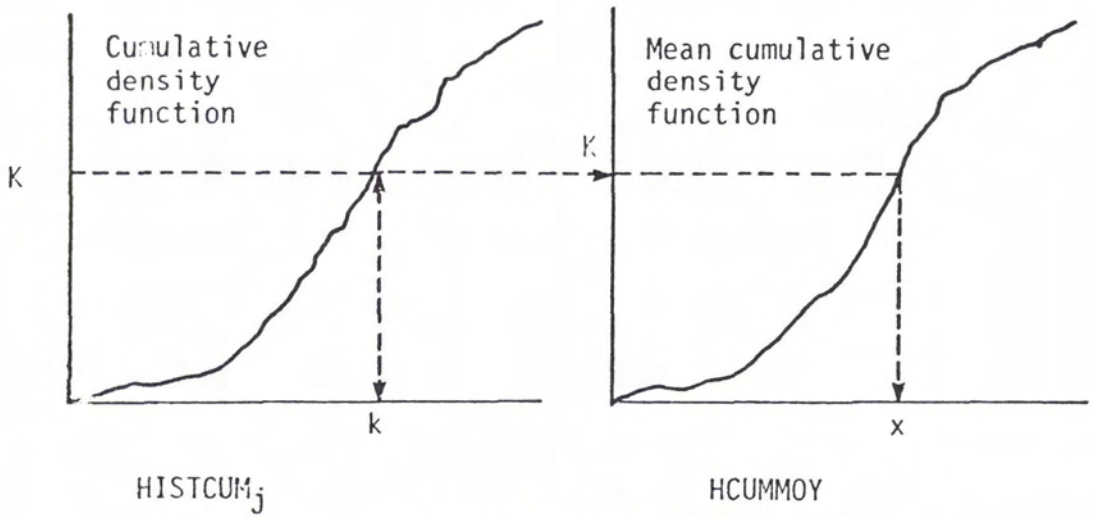

FIG. 1. Relative detector calibration method.

TABLE 5. TOULOUSE A-TYPE IMAGE MEAN DIFFERENCES BETWEEN EACH SINGLE DETECTOR AND THE MEAN DETECTOR (UNITS = GRAY LEVELS)

	Bands						
Detectors	1	2	3	4	5	6	7
D16	−0.2	−0.5	−0.2	0.6	−0.4	0.8	0.6
D15	0.	0.3	−0.3	0.1	0.4		0.1
D14	0.4	0.1	0.2	−0.2	0.1		0.3
D13	−0.3	0.9	0.	0.2	−0.2		−0.2
D12	0.9	0.7	0.8	0.3	−0.8	−1.3	0.1
D11	−0.1	0.6	0.3	−1.	−0.7		0.3
D10	0.9	0.3	0.1	0.2	0.7		0.
D9	0.4	0.3	0.4	0.1	0.		0.4
D8	1.	0.2	0.3	0.1	−0.4	1.3	−0.5
D7	0.4	−0.2	−0.3	−0.3	−0.4		0.1
D6	−0.1	−0.7	−0.1	0.6	0.1		0.4
D5	−0.5	−1.	0.3	0.4	0.9		−0.2
D4	−0.7	0.3	−0.3	−0.6	0.5	−0.8	−0.3
D3	−0.1	−0.3	0.	0.4			−0.2
D2	−0.7	−0.9	−1.1	−0.8	0.3		−1.
D1	−1.1	0.8	0.3	0.1	0.		−0.4
Levels n1 n2	36 to 65	13 to 32	10 to 34	9 to 48	3 to 82	36 to 116	1 to 40

image. On the Mississippi A-type image, we found that detector 3 of band 5 is simply a copy of detector 4 of band 5, and detector 4 of band 2 is a copy of detector 5 of band 2. Though it seems quite difficult to draw global conclusions from computations concerning different scenes at very different dates, the detectors may have suffered consistent changes in the course of time (and it seems that these images have been preprocessed in different ways: dead detectors replaced by neighbors in the Mississippi A-type scene, not replaced in the Toulouse A-type image, and unpredictably preprocessed for the Lukeville A-type scene), and the effects of scan-correlated level shifts reported by Malila (1984) and Murphy (1984) may confound these computations.

We shall, however, give some conclusions drawn *from detector calibration computations*. The largest mean differences between each single detector and the mean detector appear in the primary focal plane bands (bands 1, 2, 3, and 4 of A-type scenes of Toulouse, Mississippi, and Lukeville).

The A-type image of Mississippi (Table 6) gives

TABLE 6. MISSISSIPI A-TYPE IMAGE MEAN DIFFERENCES BETWEEN EACH SINGLE DETECTOR AND THE MEAN DETECTOR (UNITS = GRAY LEVELS)

	Bands						
Detectors	1	2	3	4	5	6	7
D16	−0.5	0.1	0.2	−0.3	−0.2	−0.6	0.1
D15	0.2	0.5	−0.4	−0.5	0.3		0.
D14	−0.3	−0.1	−0.1	−0.5	−0.1		−0.2
D13	0.3	−0.3	0.3	−0.3	0.3		0.2
D12	0.2	−0.2	0.1	0.2	0.	0.6	0.4
D11	0.2	−0.1	0.1	−0.2	0.3		0.
D10	0.9	−0.3	0.6	−0.1	0.1		−0.1
D9	−0.1	−0.3	−0.2	−0.1	0.1		−0.2
D8	0.1	−0.3	0.7	0.1	−0.1	−0.8	0.1
D7	0.3	0.	0.5	0.	−0.1		−0.1
D6	0.4	0.2	0.1	0.	−0.1		0.
D5	−0.2	0.3	−0.3	0.	0.1		0.1
D4	−0.5	0.3	0.3	0.2	−0.3	0.8	−0.1
D3	−0.2	−0.2	−0.1	0.	−0.3		−0.3
D2	0.2	0.2	0.	0.3	−0.3		−0.2
D1	0.3	−0.3	−0.8	0.	0.		0.2
Levels n1 n2	70 to 150	25 to 80	21 to 100	20 to 150	21 to 100	61 to 160	1 to 90

TABLE 7. LUKEVILLE A-TYPE IMAGE MEAN DIFFERENCES BETWEEN EACH SINGLE DETECTOR AND THE MEAN DETECTOR (OCEANIC TARGET) (UNITS = GRAY LEVELS)

	Bands						
Detectors	1	2	3	4	5	6	7
D16	−0.3	0.4	0.3	0.2	−0.2	0.6	−0.6
D15	1.1	0.2	−0.4	0.	−0.1		−0.1
D14	0.	−0.1	−0.2	−0.3	0.1		0.2
D13	−1.1	−0.1	−0.2	−0.2	0.		0.
D12	−0.5	−0.9	−0.7	−0.3	−0.2	−0.6	0.
D11	0.9	−1.	−0.5	0.	0.1		0.
D10	0.3	−1.3	−0.3	0.2	0.		0.6
D9	−1.2	0.2	0.1	0.4	0.		−0.1
D8	−0.3	0.3	0.1	0.	0.2	0.5	0.
D7	−1.1	0.8	0.3	0.4	0.		0.1
D6	−0.2	0.8	0.6	0.4	0.		0.3
D5	−0.9	1.	0.3	0.1	−0.1		0.
D4	−0.5	0.4	0.1	−0.2	0.	−0.8	0.1
D3	1.2	−0.3	0.3	0.	0.3		0.3
D2	0.1	0.5	0.4	0.	0.4		0.3
D1	−1.4	0.6	0.2	0.	−0.2		0.1
Level n1 n2	40 to 60	16 to 45	11 to 40	6 to 30	2 to 21	97 to 116	0 to 19

no mean difference higher than 1.0 or less than −1.0 gray level. However, if we look at each detector's complete lookup table, we find that for detector 4 band 1, some values are less than −1.0, for detector 10 band 1, some values are higher than 1.0 and for detector 1 band 2 some values are less than −1.2. In the A-type Toulouse scene (Table 5) we found seven differences higher than 1.0 or less than −1.0 gray level for:

- detectors 1 and 8 of band 1
- detector 2 of band 3
- detector 11 of band 4
- detectors 2 and 3 of band 6
- detector 2 of band 7.

In the special case of the Lukeville A-type scene (unfortunately it has not been possible to further investigate this scene) we did our lookup table computations on a homogeneous part of the image (sea) which had a restricted range of gray levels (see Table 7). It is quite obvious that only some detectors for bands of the primary focal plane are out of TM specifications:

- detectors 1, 3, 7, 9, 13, 15 of band 1
- detectors 5, 10, 11 of band 2.

This is quite evident if we look at primary focal plane bands 1 and 2 where severe striping appears in the oceanic part of the image.

In addition to the above-mentioned detectors whose mean differences from the mean detector absolute value are greater than or equal to 1.0 gray level, we mention the following detectors whose mean difference is low but which give differences greater than 1 (or less than −1) in some thin ranges of gray levels (denote by $D_i B_j$ the detector i of band j):

- Toulouse scene: D12B1, D5B2, D8B4, D1B7, D2B7, D16B7
- Mississippi scene: D4B1, D10B1, D1B2, D2B2, D9B2, D1B3, D2B4

Bright Target Detector Saturation. This phenomenon is quite obvious in band 1 and somewhat apparent in band 2. This saturation of all dectectors leads to severe striping when viewing snow (or bright clouds), as in the Toulouse scene. Looking at the band 1 image, it clearly appears that the detector's response recovery is very slow and may last for more than 1,000 pixels. However, even if the snow fields are surrounded by a relatively complex area, radiometrically speaking, we can see that the entire duration of saturation is about 200 pixels long (Figure 2).

CONCLUDING REMARKS

Intraband consecutive line-to-line misregistrations are concentrated near columns 1500 and 4500 and are probably correlated with mirror scan profile, but the percentage of line-to-line misregistrations between −0.3 and +0.3 IFOV is always higher than 90 percent in A-type and P-type images, which agrees with TM specifications. Our results do not agree with TM specifications, however, for band-to-band misregistration between focal planes and with band 6 for A-type and P-type images, and for the P-type Mississippi image, and all computations involving band 5.

Concerning radiometric calibration, it is quite difficult to conclude anything because the images are of very different dates; however, some detectors seem to be under TM specifications, and two detectors are dead. The bright target saturation phenomenon is very severe for bands 1 and 2.

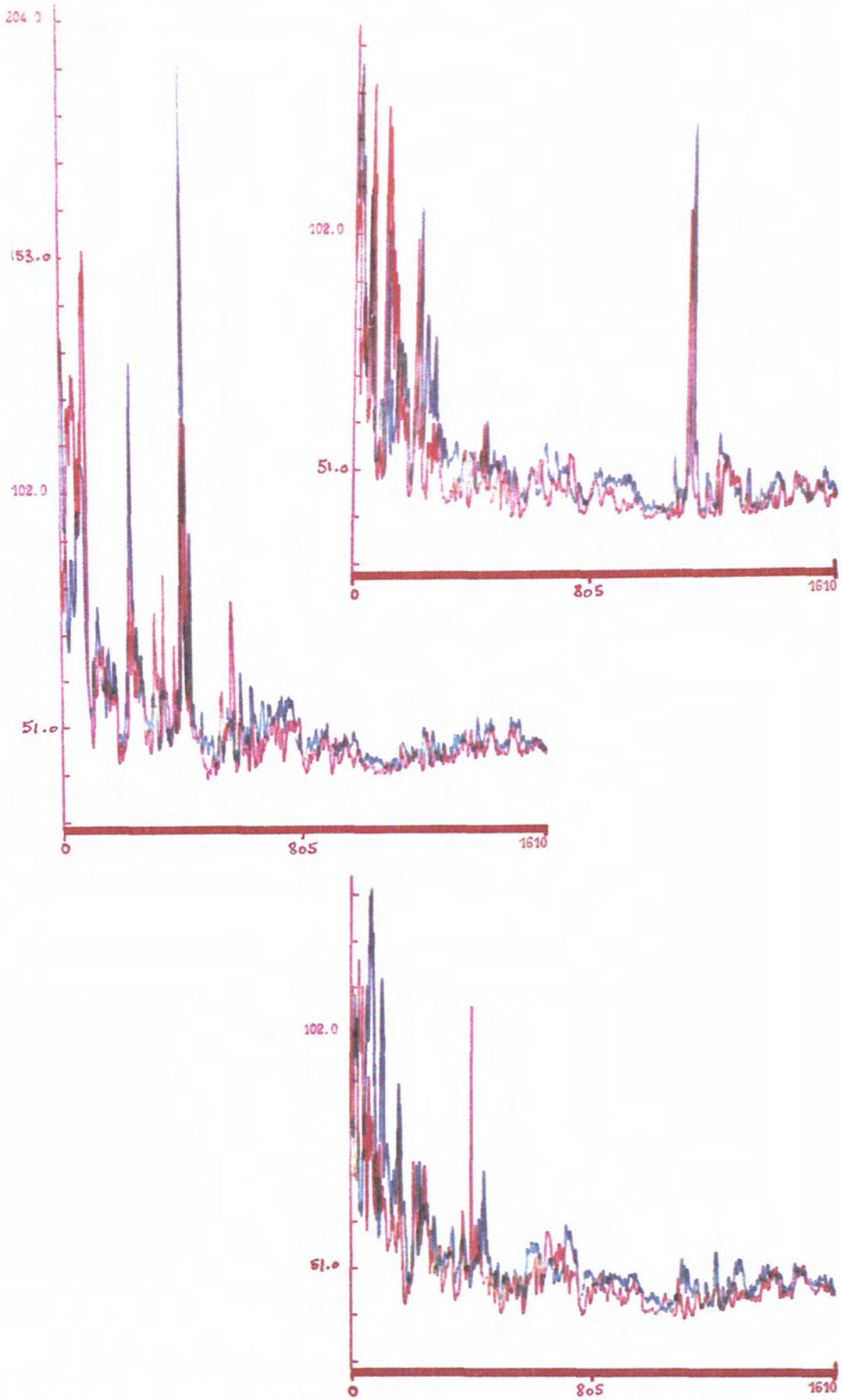

FIG. 2. Bright target saturation along 1600 pixels (band 1) for three consecutive forward-reverse scans pairs (red: forward scan mean detector profile; blue: reverse scan mean detector profile).

REFERENCES

Anuta, P. E., Bartolucci, L. A., Dean, M. E., Lozano, D. F., Malaret, E., McGillen, C. D., Valdes, J. A., and Valenzuela, C. R., 1984. Landsat-4 MSS and Thematic Mapper data quality and information content analysis: *IEEE Transactions on Geoscience and Remote Sensing*, v. GE-22, no. 3 (May), pp. 222-236.

Bernstein, R., Lotspiech, J. B., Myers, H. J., Kolsky, H. G., and Lees, R. D., 1984. Analysis and processing of Landsat-4 Sensor data using advanced Image processing techniques and technologies: *IEEE Transactions on Geoscience and Remote Sensing*, v. GE-22, no. 3 (May), pp. 192-221.

Jeansoulin, R., 1980. Automated image to image registration, a way to multitemporal analysis of remotely sensed data: in *DIGITAL IMAGE PROCESSING: Proceedings of the NATO Advanced Study Institute* (June 23–July 4), (edited by J. C. Simon and R. M. Harralick), D. Reidel Publishing Company.

Malila, W. A., Metzler, M. D., Rice, D. P., and Crist, E. P., 1984. Characterization of LANDSAT-4 MSS and TM Digital image data: *IEEE Transactions on Geoscience and Remote Sensing*, v. GE-22, no. 3 (May), pp. 177-191.

Murphy, J. M., Butlin, T., Duff, P. F. and Fitzgerald, A. J., 1984. Revised radiometric calibration technique for Landsat-4 TM data: *IEEE Transactions on Geoscience and Remote Sensing*, v. GE-22, no. 3 (May), pp. 243-250.

Wrigley, R. C., Card, D. H., Hlavka, C. A., Hall, J. R., Mertz, F. C., Archwamety, C., and Schowengerdt, R. A., 1984. Thematic Mapper Image Quality: Registration, Noise and Resolution: *IEEE Transactions on Geoscience and Remote Sensing* v. GE-22, no. 3 (May), pp. 263-271.

Instrumentation for Optical Remote Sensing from Space

Cannes, France
25-29 November 1985

This Conference—organized by the Association Nationale de la Recherche Technique (ANRT) and the International Society for Optical Engineering (SPIE) and sponsored, with others, by the American Society for Photogrammetry and Remote Sensing—will emphasize new or developing instrumentation concerning the sensing of atmospheric constituents, astronomical objects, and the Earth's surface.

For further information please contact

SPIE
P.O. Box 10
Bellingham, WA 98227-0010

Third International Colloquium Spectral Signature of Objects in Remote Sensing

Les Arcs, Bourg-Saint-Maurice, France
16-20 December 1985

This Colloquium of Working Group 3, Commission VII, of the International Society for Photogrammetry and Remote Sensing—sponsored by the Association Québécoise de Télédétection, Canadian Remote Sensing Society, European Association of Remote Sensing Laboratories, I.E.E.E. Geoscience and Remote Sensing Society, Remote Sensing Society, and Société Française de Photogrammétrie et de Télédétection and supported by the Centre National d'Etudes Spatiales (C.N.E.S.), European Space Agency (E.S.A.), and Institut National de la Recherche Agronomique—has as its objective to reunite specialists from different fields of study—physicists, agronomists, foresters, hydrologists, oceanologists—who are interested in analyzing relationships between specific properties of a target (vegetative canopy, soil, rocks, water surfaces, snow, ice, etc.) and its spectral characteristics in different wavelength bands from ultraviolet to microwaves.

For further information please contact

M. Gerard Guyot or M. Michel Verbrugghe
INRA Bioclimatologie
B.P. 91
F. 84140 Montfavet, France
Tele. (90) 88 91 45